Characterization of Phospholipid Bilayer Formation on a Thin Film of Porous SiO2 by Reflective Interferometric Fourier Transform Spectroscopy (RIFTS)

ARTICLE *in* LANGMUIR · APRIL 2012

Impact Factor: 4.46 · DOI: 10.1021/la301085t · Source: PubMed

7 AUTHORS, INCLUDING:

Stephanie Pace
University of Angers
14 PUBLICATIONS **160** CITATIONS
SEE PROFILE

Bastien Seantier
Université de Bretagne Sud
22 PUBLICATIONS **434** CITATIONS
SEE PROFILE

Langmuir

Article

pubs.acs.org/Langmuir

Characterization of Phospholipid Bilayer Formation on a Thin Film of Porous SiO_2 by Reflective Interferometric Fourier Transform Spectroscopy (RIFTS)

Stéphanie Pace,[†] Bastien Seantier,[‡,§,⊥] Emmanuel Belamie,[†] Nicole Lautrédou,[§] Michael J. Sailor,[∥] Pierre-Emmanuel Milhiet,[‡,§] and Frédérique Cunin*[,†]

[†]Institut Charles Gerhardt Montpellier, UMR 5253 CNRS-ENSCM-UM2-UM1, Matériaux Avancés pour la Catalyse et la Santé, Ecole Nationale Supérieure de Chimie de Montpellier, 8 rue de l'Ecole Normale, 34296 Montpellier, France.

[‡]Institut National de la Santé et de la Recherche Médicale, Unité 1054, 34090 Montpellier, France

[§]Centre National de la Recherche Scientifique, UMS 3426/MRI, Centre de Biochimie Structurale, 34090 Montpellier, France

[∥]Department of Chemistry and Biochemistry, m/c 0358, University of California—San Diego, 9500 Gilman Drive, La Jolla, California 92093-0358, United States

Supporting Information

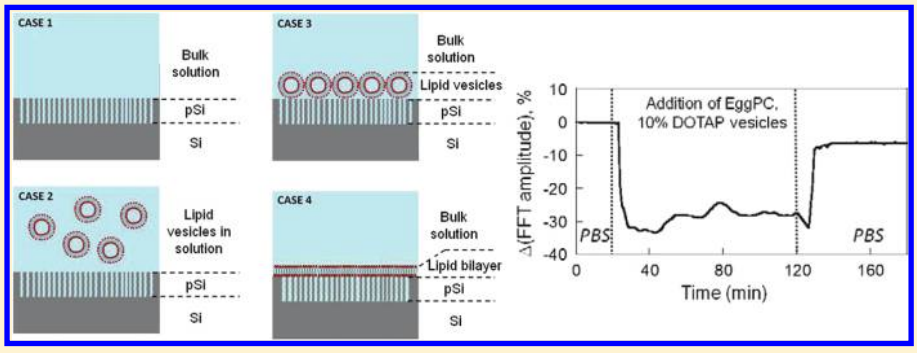

ABSTRACT: Classical methods for characterizing supported artificial phospholipid bilayers include imaging techniques such as atomic force microscopy and fluorescence microscopy. The use in the past decade of surface-sensitive methods such as surface plasmon resonance and ellipsometry, and acoustic sensors such as the quartz crystal microbalance, coupled to the imaging methods, have expanded our understanding of the formation mechanisms of phospholipid bilayers. In the present work, reflective interferometric Fourier transform spectrocopy (RIFTS) is employed to monitor the formation of a planar phospholipid bilayer on an oxidized mesoporous Si ($pSiO_2$) thin film. The $pSiO_2$ substrates are prepared as thin films (3 μm thick) with pore dimensions of a few nanometers in diameter by the electrochemical etching of crystalline silicon, and they are passivated with a thin thermal oxide layer. A thin film of mica is used as a control. Interferometric optical measurements are used to quantify the behavior of the phospholipids at the internal (pores) and external surfaces of the substrates. The optical measurements indicate that vesicles initially adsorb to the $pSiO_2$ surface as a monolayer, followed by vesicle fusion and conversion to a surface-adsorbed lipid bilayer. The timescale of the process is consistent with prior measurements of vesicle fusion onto mica surfaces. Reflectance spectra calculated using a simple double-layer Fabry–Perot interference model verify the experimental results. The method provides a simple, real-time, nondestructive approach to characterizing the growth and evolution of lipid vesicle layers on the surface of an optical thin film.

INTRODUCTION

Biological membranes are essential constituents of living cells. They form a protective barrier, act as a filter against extracellular insults, and mediate cellular communication with the extracellular environment including the matrix and other cells. Membranes are composed of lipids and proteins organized in a bilayer with variable lipid constituents within and between the two leaflets. Biological membranes are also highly dynamic molecular assemblies. Because of their complexity, several artificial systems have been developed to study membranes and membrane properties, in particular, unilamellar vesicles with sizes ranging from tens of nanometers (small unilamellar vesicles) to several micrometers (giant unilamellar vesicles)[1] and supported lipid bilayers (SLB).[2−6] Mineral oxides such as mica, oxidized silicon wafers, glass, and quartz are substrates traditionally used as supports for lipid bilayers because they are planar, chemically inert, and possess a hydrophilic surface. Classical methods of characterizing artificial supported lipid bilayers on mineral oxides include imaging

Received: November 1, 2011

   dx.doi.org/10.1021/la301085t | Langmuir XXXX, XXX, XXX−XXX

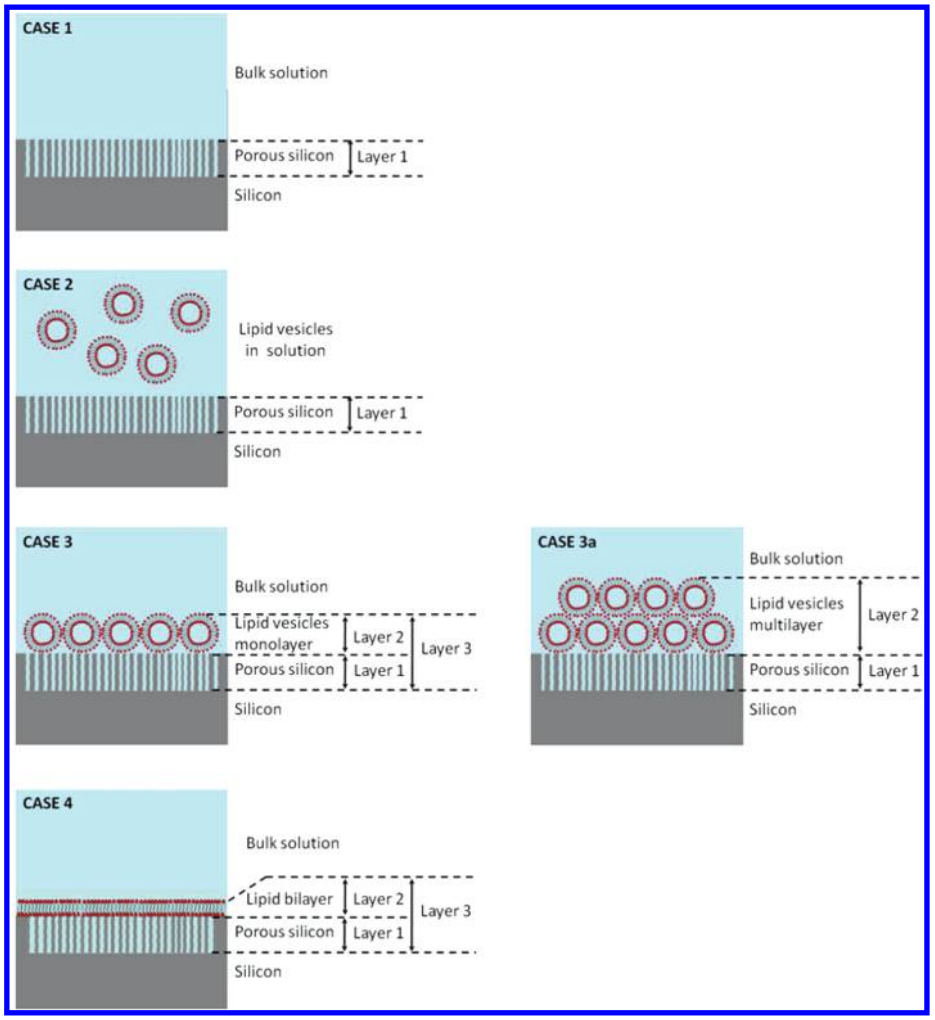

Figure 1. Illustration of different possible stages for lipid vesicle deposition and lipid bilayer formation on a $pSiO_2$ surface. Case 1: a bare $pSiO_2$ surface in aqueous buffer. Case 2: an uncoated bare $pSiO_2$ surface in a solution of lipid vesicles in aqueous buffer. Case 3: a $pSiO_2$ surface coated with a single layer of lipid vesicles in aqueous buffer. Case 3a: $pSiO_2$ coated with a multilayer of lipid vesicles in aqueous buffer. Case 4: $pSiO_2$ coated with a lipid bilayer in aqueous buffer.

techniques such as atomic force microscopy (AFM) and fluorescence optical microscopy.[7,8] The use of surface-sensitive methods including surface plasmon resonance (SPR)[9,10] and ellipsometry and/or acoustic methods such as the quartz crystal microbalance with dissipation monitoring (QCM-D),[11−14] coupled to the imaging methods, has expanded the understanding of formation mechanisms of phospholipid bilayers. In particular, Brisson and co-workers have established several possible pathways of vesicle deposition and bilayer formation on flat silica supports that depend on the charge of the lipid vesicles, using AFM and QCM-D.[15] This work followed initial SPR and QCM-D studies of Kasemo and co-workers, who suggested that the formation of a lipid bilayer on flat silica is preceded by the adsorption of intact lipid vesicles.[16,17]

In the present work, optical interferometry is employed to monitor the formation of a planar SLB on an oxidized mesoporous Si thin film ($pSiO_2$). The material, prepared by the electrochemical etching of crystalline silicon in hydrofluoric acid, contains nanometer-scale pores whose dimensions are controlled by the synthesis.[18−21] When properly functionalized, $pSiO_2$ has proven to be a suitable planar support for SLBs.[22,23] The reflectance spectrum obtained from a $pSiO_2$ layer consists of high-fidelity fringes due to thin-film Fabry−Perot interference. The fast Fourier transform (FFT) of this spectrum yields a single peak whose position and intensity correlate with the refractive index of the porous film. The extraction of the refractive index and thickness of the porous film by FFT is referred to as the reflective interferometric Fourier transform spectrocopy (RIFTS) method.[19,20] The RIFTS technique has been shown to be an efficient and sensitive means of monitoring events that occur at the porous silicon/liquid interface. In this work, we show that the method can be used to characterize the formation of a phospholipid bilayer on the external surface of a planar $pSiO_2$ substrate.

The approach in this work consisted of simulating the $pSiO_2$/SLB system as a double-layer Fabry−Perot system whose reflectance properties (including the amplitude and position of the FFT peaks) were then calculated, considering the refractive index and thickness of each layer. Four cases were considered for the simulation, which illustrate possible states during the phospholipid bilayer formation process (Figure 1). The steps in vesicle deposition and bilayer formation have been described in the literature for lipid vesicles of low charge exposed to flat silica supports.[8,15−17] After the introduction of a vesicle solution into the substrate (case 1 → 2), adsorption of the intact vesicles to the $pSiO_2$ surface occurs (case 2 → 3).

dx.doi.org/10.1021/la301085t | *Langmuir* XXXX, XXX, XXX−XXX

This is followed by the transformation of the adsorbed vesicle layer to a lipid bilayer (case 3 → 4). In addition, the hypothetical case of the formation of vesicle multilayers was considered (case 3 → 3a). Experimental optical measurements were performed in situ during the deposition of lipid vesicles on a lightly oxidized porous silicon film using a CCD spectrometer. The experimental data compare favorably with the calculated spectra, indicating that the approach can provide nondestructive, real-time insight into the lipid fusion process.

MATERIALS AND METHODS

Synthesis of Porous Silicon Films. Single-crystal, polished p^{++}-type silicon wafers (boron doped, 0.0008−0.0012 Ω.cm resistivity, (100)-oriented) from Siltronix Inc. were first cleaned in boiling absolute ethanol (Sigma-Aldrich) for 30 min. They were then cleaned following the RCA protocol: the wafers were treated in RCA bath 1 ($H_2O/NH_4OH/H_2O_2$ = 5:1:1 volume ratio) at 80 °C for 15 min, rinsed with deionized water, and then immersed in RCA bath 2 ($H_2O/HCl/H_2O_2$ = 5:1:1 volume ratio) at 80 °C for 15 min, rinsed with deionized water and ethanol, and finally dried in a stream of dry argon.

Porous Si films were prepared by electrochemical etching of the cleaned wafers in a 3:1 (volume ratio) solution of 48% aqueous hydrofluoric acid and ethanol (Sigma-Aldrich). The Si wafers with an exposed area of 0.16 cm^2 (diameter = 4.5 mm) were placed in contact with a strip of aluminum foil and mounted in a Teflon etching cell with a platinum counter electrode. The wafers were etched at a constant current density of 22.5 mA/cm^2 for 325 s.

To render them hydrophilic, the freshly prepared porous silicon films were thermally oxidized at 450 °C for 2 h in a muffle (box) furnace in air (Nabertherm, B170, 30−3000 °C) and then immersed in a 1 M NaOH (Sigma-Aldrich) solution for 2 min, rinsed extensively with deionized water and ethanol, and finally dried in a stream of dry argon. The oxidized porous silicon ($pSiO_2$) films were stored and transported in plastic tubes filled with ethanol to prevent contamination and dust deposition.

Synthesis of Large Unilamellar Vesicles. Multilamellar vesicles (MLV) were prepared from 10 mM stock solutions of either L-α-phosphatidylcholine (from chicken eggs) (eggPC), dipalmitoylphosphatidylcholine (DPPC), or 1,2-dioleoyl-3-trimethylammonium-propane (DOTAP, Avanti) in chloroform/methanol (2:1). A 0.5% aqueous solution of dioleoyl-*sn*-glycero-3-phosphoethanolamine-*N*-(fluorescein isothiocyanate) (DOPE-FITC) was added to the lipid mixture to enable fluorescence imaging. After the solvent was evaporated under nitrogen, the lipids were suspended in a phosphate-buffered saline (PBS, Invitrogen, pH 7.4) solution under an argon atmosphere. The final concentration of lipids was 1.25 mM. The purity of the phospholipids was verified by thin layer chromatography. Large unilamellar vesicles (LUV) of 100 nm in size were generated at 65 °C by extrusion through polycarbonate membranes (Avanti).

Preparation of Mica Thin Films. Thin films of mica displaying interference fringes in their reflectivity spectra were prepared by manual cleavage of the appropriate thickness of mica sheets (Goodfellow).

Interferometric Reflectance Spectral Measurements. White light from a tungsten lamp (Ocean Optics R-LS-1) was fed through one end of a bifurcated fiber-optic cable and focused through a lens onto the surface of the $pSiO_2$ film at normal incidence. The light source was focused onto the center of the sample surface with a spot size that was approximately 1.5 mm in diameter. Light reflected from the film was collected through the same optics, and the distal end of the bifurcated fiber optic cable was input into a CCD spectrometer (Ocean Optics S-2000). Reflectivity spectra were recorded in the wavelength range of 600−1000 nm with a spectral acquisition time of 0.1 s. Typically, 100 spectral scans (10 s total integration time) were averaged. To obtain the Fourier transform of the resulting spectrum, the *x* axis was inverted and a linear interpolation was applied such that the data were spaced evenly in units of nm^{-1}. A Hanning window was applied to the spectrum and was redimensionalized to 4096 data points and zero padded to the power of 2. A discrete fast Fourier transform using a multidimensional fast prime factor decomposition algorithm from the Wavemetrics Inc. (www.wavemetrics.com) IGOR program library (FFT) was applied.

Experiments were carried out in a custom-made aqueous flow cell at room temperature. The $pSiO_2$ sample was placed under vacuum in a desiccator for 30 min before mounting in the flow cell. A solution of aqueous PBS buffer (pH 7.4) was introduced at a flow rate of 100 μL/min. A solution of lipid vesicles in the same buffer was then infused into the flow cell. Two minutes after the introduction of the vesicles, the flow was stopped for 40 to 80 min. A rinsing solution of PBS was then introduced at a flow rate of 50 μL/min. Interference spectra were collected every 1 min.

Spectral Calculations. Reflectance spectra were calculated using a simple double-layer Fabry−Perot interference model after the treatment of McLeod.[24] The model assumes a single reflection per layer (no multiple reflections), and the layers are composed of $pSiO_2$, a lipid bilayer, or a lipid vesicle layer(s) as outlined in Figure 1. The equation describing the reflectance spectrum for the double-layer structure is given by

$$R(\lambda) = [\rho_a^2 + \rho_b^2 + \rho_c^2] + 2\rho_a\rho_b \cos(2d_1) + 2\rho_b\rho_c \cos(2d_2) + 2\rho_a\rho_c \cos(2(d_1 + d_2)) \quad (1)$$

where d_1 and d_2 are the phase relationships described by

$$d_1 = \frac{2\pi n_1 L_1}{\lambda}$$

and

$$d_2 = \frac{2\pi n_2 L_2}{\lambda}$$

n_1, n_2, L_1, and L_2 are the refractive indices of layers 1 and 2 and the thickness (in nm) of layers 1 and 2, respectively. λ is the wavelength of incident light.

The terms ρ_a, ρ_b, and ρ_c represent the refractive index contrast between layers, defined as

$$\rho_a = \frac{n_{soln} - n_2}{n_{soln} + n_2}$$

$$\rho_b = \frac{n_2 - n_1}{n_2 + n_1}$$

$$\rho_c = \frac{n_1 - n_{Si}}{n_2 + n_{Si}}$$

where n_{soln}, n_{Si}, and n_1 are the refractive indices of the solution, of bulk silicon, and of the $pSiO_2$ layer, respectively.

The quantity n_2 represents the refractive index of the liposome single layer, liposome multilayer, or lipid bilayer on the surface of the $pSiO_2$ film.

For each case described in Figure 1, the calculated reflectance spectrum consists of interference fringes due to thin-film Fabry−Perot interference in the three layers defined in Figure 1. The refractive index and the thickness of these individual components were extracted by applying a fast Fourier transform (FFT) to the calculated reflectance spectrum as described above.[19,20] The Fourier transform of the spectrum yields a peak whose position on the *x* axis corresponds to the value 2*nL* (the effective optical thickness for a reflection mode experiment) in the Fabry−Perot relationship given in eq 2

$$m\lambda = 2nL \quad (2)$$

where *m* is an integer, *L* is the thickness of the $pSiO_2$ layer, *n* is the average refractive index, and λ is the wavelength of the incident light. The amplitude or position of each peak in the FFT was then quantified using a least-squares peak-fitting routine consisting of either a Gaussian function or an interpolation of the smoothed first and second derivatives of the waveform.

dx.doi.org/10.1021/la301085t | *Langmuir* XXXX, XXX, XXX−XXX

Determination of Refractive Indices of Liquids Used in the Study. Refractive indices of phosphate-buffered PBS and of lipid vesicle suspensions (eggPC in PBS, 1.25 mM) were measured using an ATAGO refractometer.

Determination of the Parameters Used in the Simulation of Optical Properties of Lipid Bilayers and Lipid Vesicle Single Layers. The values of the refractive indices for bulk silicon and for a lipid bilayer of eggPC, 3.8 and 1.45, respectively, were taken from the literature.[19,25]

Liposomes were modeled as spherical vesicles, 20.6% (by volume) lipid and 79.4% PBS buffer. A single layer of liposomes was assumed to pack with a hexagonal close packing (HCP) efficiency of 74%, so the composition of a layer of liposomes was modeled as 15.2% lipid and 84.8% PBS buffer. The Bruggeman effective medium approximation was then used to calculate the average refractive index of an individual vesicle and a monolayer or multilayer of vesicles; the results of the calculations are given in Table 1. The refractive index of the $pSiO_2$ layer containing buffer (n_1) was determined from the measured refractive index of PBS and an experimentally approximated value of the refractive index of the silicon/silicon oxide skeleton in the $pSiO_2$ layer. The porosity of the $pSiO_2$ film was determined to be 55% (from cryogenic nitrogen adsorption–desorption measurements). The value of the refractive index of the $pSiO_2$ skeleton was determined from the best fit of the spectral reflectance data, which yielded a value of 1.9 for this component. The refractive index of the skeleton is modeled as a single, wavelength-independent value corresponding to the index of a partially oxidized film (one containing both crystalline Si and SiO_2). The average index of the $pSiO_2$ layer (Table 1), containing both the $pSiO_2$ skeleton and the PBS buffer solution, was then determined using the Bruggeman effective medium approximation.

Table 1. Parameters Used in Simulation of Optical Properties of Lipid Bilayers and Lipid Vesicle Single Layers on $pSiO_2$ Films

component	thickness (nm)	index of refraction	comment
buffer solution[a]	N/A	1.3348	case 1: refractometer measurement
porous silicon layer + buffer solution[b]	3000	1.58	case 1-4: geometrical calculation based on Bruggeman approximation.
buffer solution containing lipid vesicles	N/A	1.3349	case 2: refractometer measurement
lipid vesicle (isolated)	100	1.3585	geometrical calculation based on Bruggeman approximation.
lipid vesicle single layer	100	1.3523	case 3: geometrical calculation based on Bruggeman approximation.
lipid bilayer	3.7	1.45	case 4: surface plasmons calculation from ref 26
lipid vesicle multilayer	500	1.3523	case 3a: geometrical calculation based on Bruggeman approximation.

[a]Phosphate-buffered saline solution. [b]Average refractive index of a porous Si layer with PBS buffer filling the pores. The porous Si layer was thermally oxidized (450 °C, 2 h) and then treated with aqueous NaOH (1 M) prior to measurement.

RESULTS AND DISCUSSION

Simulated Reflectance Spectra of the Different Stages of Vesicle Adsorption. Reflectance spectra were simulated for the five hypothetical cases illustrated in Figure 1, corresponding to different stages of lipid vesicle deposition and bilayer formation on a $pSiO_2$ surface. Reflectance spectra were calculated using a simple double-layer Fabry–Perot interference model after the treatment of McLeod.[24] The layers were composed of $pSiO_2$ (referred to as layer 1), a lipid vesicle layer, or a lipid bilayer (referred to as layer 2). The refractive index and the thickness of the various components used in the simulations are given in Table 1.

Case 2 is expected to be similar to case 1 on the basis of the similarity in the refractive indices of the pure buffer and the buffer containing vesicles. The simulation assumes that no intrusion of lipid or liposome into the pores of the $pSiO_2$ film occurs during the experiment, thus the value of n_1 (refractive index of the $pSiO_2$ layer) was held constant. This assumption is supported by prior experimental measurements on $pSiO_2$ films prepared under similar conditions of current density and HF concentration,[22] suggesting that the pore diameters in the present samples are too small to allow for significant infiltration of the lipid vesicles. For case 4, we assumed that the optical effect of the very thin (1 to 2 nm) water layer between the lipid bilayer and the top of the $pSiO_2$ sample was negligible.[26,27] Finally, we have not considered a possible intermediate step between cases 3 and 4, consisting of a "pancake-like" vesicle deformation before rupture, which has been proposed by Brisson and co-workers for LUVs (large unilamellar vesicles) adsorbed on mica.[7] Representative reflectance spectra for cases 1, 3, and 4 in Figure 1 are presented in Figure 2a. The spectra correspond to a single-layer $pSiO_2$ film coated with a close-packed single layer of lipid vesicles (case 3), the same $pSiO_2$ layer coated with a single lipid bilayer (case 4, corresponding to a situation in which the lipid vesicles have ruptured into a bilayer on the porous Si surface). The spectrum of a multilayer of lipid vesicles coated on a single-layer $pSiO_2$ film is also included as a separate case (3a). In all cases, the system is assumed to be immersed in aqueous buffer (PBS). For comparison, a spectrum of a bare single layer of $pSiO_2$ immersed in PBS is presented (case 1).

The differences between the spectra representing cases 3, 3a, and 4 in Figure 1 are not particularly distinguishable from the bare, uncoated $pSiO_2$ surface (case 1). A fast Fourier transform (FFT) algorithm, similar to the one used on the experimental reflectivity spectra (in Materials and Methods), was applied to the simulated spectral data. Three peaks are expected in the FFT of the spectrum of a double-layer structure, and their positions correspond to the quantity $2nL$ for layer 1, layer 2, and the combination layer 1 + layer 2, respectively. The combination (layer 1 + layer 2) is designated as layer 3 in Figure 1. The FFT spectra are presented in Figure 2b. The Fourier transforms of the spectra are more informative. The positions of the FFT peaks along the x axis are equal to the value of 2 nL for a particular layer designated in Figure 1. The major peak shown in Figure 2b corresponds to layer 1. We observed that the intensity of the peak corresponding to layer 3 is fairly weak, even in case 3a, where the lipid vesicle layer is sufficiently thick to allow the separation of peaks 1 and 3 in the FFT spectrum. In this case, only layers 1 and 3 are visible, and the amplitudes of these two FFT peaks correspond to the product of the index contrast at the interfaces corresponding to layers 1 and 3, namely, the quantities $2\rho_b\rho_c$ and $2\rho_a\rho_c$, respectively. As expected, no variation in the optical thickness ($2nL$) is observed, considering that the value of n_1 is constrained to a single value in the model. The main effect of the presence of the lipid or liposome layer is to influence the amplitude of the main peak, which corresponds to the $pSiO_2$ layer itself (layer 1). The variation in the amplitude of the FFT peak corresponding to layer 1 is shown in Figure 2c for each of the four cases. The data are presented as percent changes in amplitude, relative to case 1. The adsorption of a lipid vesicle

dx.doi.org/10.1021/la301085t | Langmuir XXXX, XXX, XXX–XXX

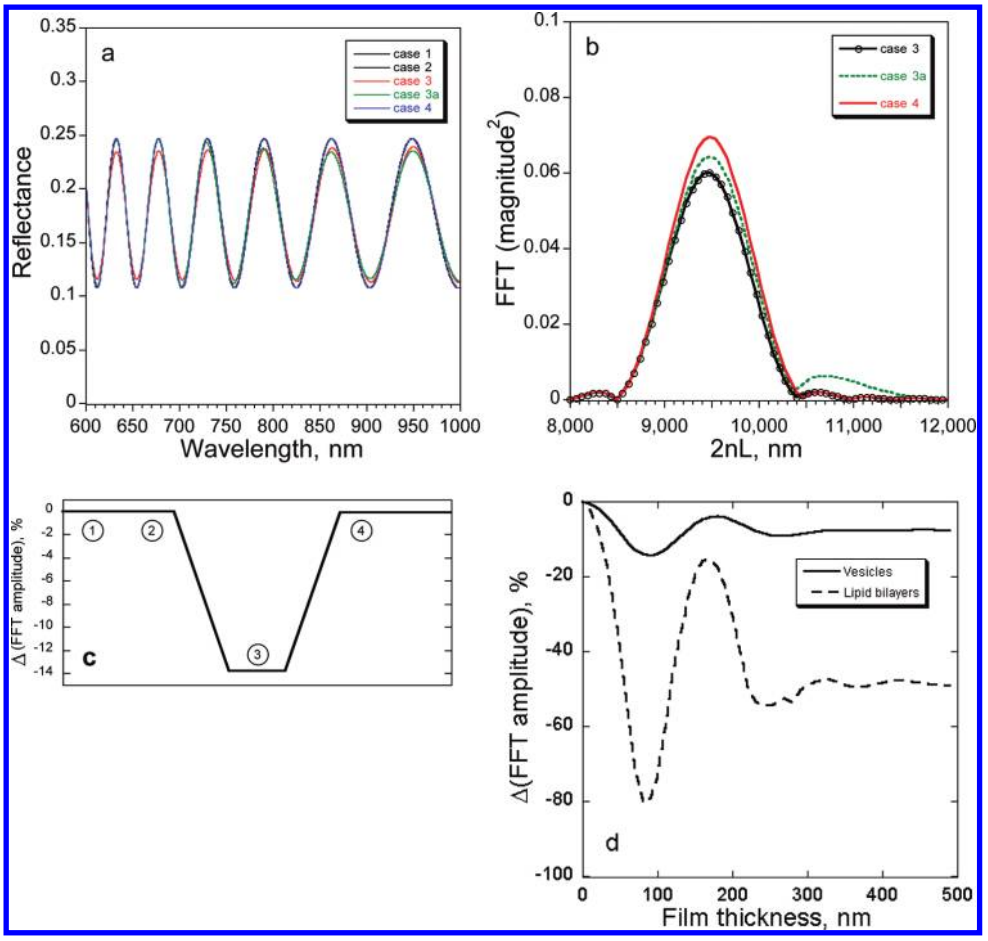

Figure 2. Simulated results obtained for the exposure of $pSiO_2$ films to several lipid coatings. (The input parameters are summarized in Table 1.) (a) Calculated reflectance spectra of porous Si samples for the cases illustrated in Figure 1. (b) Fourier transform spectra of the calculated reflectance spectra shown in a. Cases as illustrated in Figure 1. (c) Calculated percent change in the amplitude of the FFT peak from b for each case illustrated in Figure 1. (d) Calculated percent change in the amplitude of the FFT peak from b (corresponding to the index contrast at the $pSiO_2$ layer/solution interface) as a function of the film thickness, in nm, for a film composed of lipid vesicles (—) or lipid bilayers (---).

single layer onto the surface of $pSiO_2$ leads to a significant decrease in the amplitude of the FFT peak. However, the trace in Figure 2b corresponding to case 4 (i.e., the $pSiO_2$ sample coated with a 3.7-nm-thick lipid bilayer) is indistinguishable from case 1 (the $pSiO_2$ sample with no overlayer), indicating that the presence of a single lipid bilayer is not readily detected with the FFT method. Such a result was previously experimentally observed from a $pSiO_2$ thin film reflector, where no difference in the amplitude of the Rugate peak was observed after the formation of a phospholipid bilayer on the surface of the porous mirror.[22]

A second simulation was performed to discern the effect of a growing lipid bilayer or lipid vesicle layer on the amplitude of the observed peak in the FFT spectrum. The amplitude of the FFT peak as a function of the thickness of the lipid bilayer or the lipid vesicle layer is presented in Figure 2d. In this simulation, the refractive indices for each of the components are constrained to the values given in Table 1, and the thickness of the lipid bilayer or lipid vesicle layer is steadily increased to a maximum thickness of 500 nm, which corresponds to a stack of 135 lipid bilayers or 5 vesicle monolayers.

It is clear from the traces in Figure 2d that as the thickness of either layer increases, the intensity of the FFT peak exhibits a damped oscillatory function. This oscillation is a function of the resolution of the FFT algorithm, which ultimately depends on the resolution of the original reflectance spectrum. In the present simulation, the resolution of the spectrum is set at ~0.4 nm, which generates an oscillation whose first minimum for all reasonable values of the refractive index corresponds to a layer thickness of ~90 nm. The frequency of the oscillation is only very weakly dependent on the refractive index. This value of 90 nm is somewhat arbitrary in that it depends on the spectral resolution of the original reflectance spectrum and not on any fundamental length scale having to do with the lipid vesicle diameter.

The main conclusion that can be drawn from this simulation is that the introduction of a layer whose refractive index lies between that of the $pSiO_2$ layer and that of the buffer solution will generate an oscillation in the intensity of the FFT peak. The amplitude of this oscillation scales with the refractive index of the coating layer; a lipid vesicle layer (n = 1.35) will generate a lower-amplitude oscillation than will a lipid bilayer (n = 1.45). The amplitude of the oscillation allows for monitoring of the evolution of a lipid vesicle monolayer or multilayer. The vesicles used in this work have a diameter of 100 nm, so the formation of an intact single layer of 100-nm-thick vesicles should produce the smallest relative amplitude value, as shown in Figure 2d. The growth of additional lipid vesicle layers will result in a slight increase in the amplitude of the FFT peak, corresponding to moving along the x axis in Figure 2d. A

dx.doi.org/10.1021/la301085t | *Langmuir* XXXX, XXX, XXX−XXX

similar effect with increased amplitude variations is expected when growing additional lipid bilayers that have a higher refractive index (1.45) than lipid vesicle layers (1.35). Because of the much smaller thickness of a single lipid bilayer (or even that of several superimposed bilayers), vesicle rupture and spreading into a bilayer is expected to generate a small change in the FFT amplitude.

Comparison of Simulated Curves with Experimental Data. To compare the predictions of the simulation with experimental data, $pSiO_2$ films were exposed to solutions of L-α-phosphatidylcholine (eggPC) and 10% DOTAP lipid vesicles in a customized flow cell, and reflectivity spectra were collected as a function of time at room temperature. Oxidized porous silicon is more chemically stable in buffer solutions than in freshly etched porous silicon, and the oxide imparts a silica-like hydrophilicity that proved to be favorable for phospholipid vesicle deposition and bilayer formation.[22] Large unilamellar vesicle (LUV) solutions were prepared under conditions favoring bilayer formation on the substrate from the fusion of adsorbed vesicles. LUVs with 100 nm diameter were made from eggPC phospholipids enriched with 10% DOTAP lipids. The DOTAP additive possesses a positively charged headgroup intended to generate favorable interactions with the negatively charged oxidized $pSiO_2$ surface in PBS (pH 7.4).[22] With a phase-transition temperature of 0 °C, eggPC was in a fluid phase at room temperature, which also favored the vesicle-to-bilayer transformation.[28] Figure S1 in the Supporting Information section displays fluorescence microscopy images and FRAP (fluorescence recovery after photobleaching) of the eggPC + 10% DOTAP + 0.5% DOPE-CF lipid bilayer supported on a thin film of $pSiO_2$. The $pSiO_2$ layer was divided into square regions 300 μm on an edge by means of a platinum mask that was photolithographically deposited on the silicon wafer prior to the etching step. Fluorescence recovery curves obtained from regions within a given square (Figure S1b) show almost total fluorescence recovery with a calculated mobile fraction (R) value of 0.94 and a diffusion coefficient value of 2.1 $\mu m^2\ s^{-1}$. This value for the diffusion coefficient is of the same order of magnitude as the estimated diffusion coefficient for a supported lipid bilayer in a fluid phase on a glass substrate.[29,30]

AFM images of $pSiO_2$ before and after deposition of the phospholipid bilayer (Figure S2) indicate that the samples have an rms roughness (0.485 nm) that is larger than that of mica (<0.1 nm) and in the same range as typical glass slides. We assume that roughness on this scale will not drastically modify the membrane behavior because the relevant dynamics of supported lipid bilayers have been shown to be preserved on glass supports.[29,30] However, the roughness is expected to influence the shape of lipid domains in the phase-separated membranes as previously observed.[22,31] The observation of holes of depth ~4.5 nm is an indication of the presence of the phospholipid bilayer on the porous silicon substrate. These data confirm that $pSiO_2$ provides a suitable planar support for fluid DOTAP-enriched PC lipid bilayers with a reasonably high substrate coverage and low pinhole density.

The interference spectrum of the $pSiO_2$ film in PBS is presented in Figure 3a. Figure 3b,c displays the time evolution of the value of $2nL$ and the intensity of the FFT peak from the $pSiO_2$ film, respectively, upon exposure to a solution of eggPC + 10% DOTAP vesicles.

No abrupt change in the value of $2nL$ was observed after the addition of the lipid vesicles (Figure 3b). This result indicates

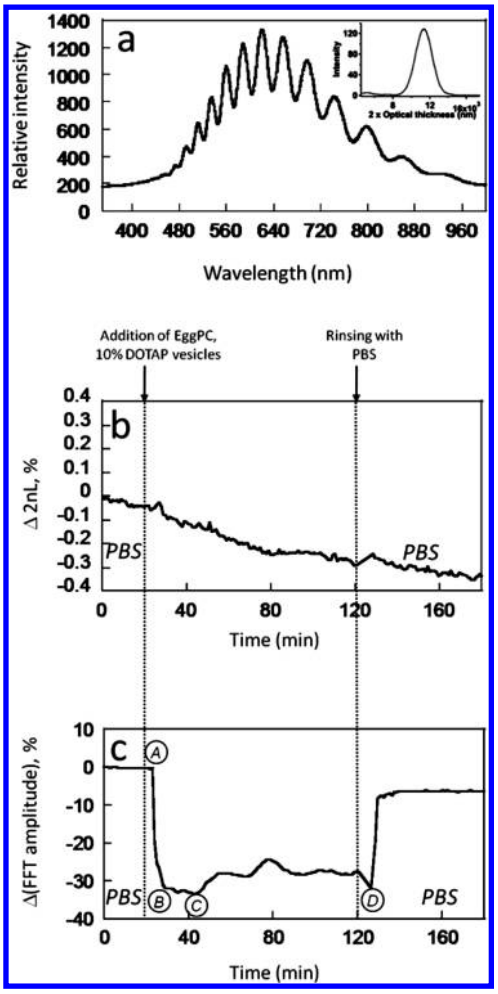

Figure 3. Experimental RIFTS data for a $pSiO_2$ film exposed to an eggPC + 10% DOTAP lipid solution. (a) Reflected light spectrum displaying interference fringes from a bare single layer film of $pSiO_2$. The $pSiO_2$ film was prepared by air oxidation at 450 °C, then treated with NaOH (1 M). The sample is immersed in pure PBS solution. The spectrum is not corrected for the instrumental response (Inset) Fourier transform of the spectrum in a. The FFT spectrum displays a single peak whose position along the x axis corresponds to the value $2nL$ for the $pSiO_2$ layer. (b) Value of $2nL$ as a function of time for the $pSiO_2$ layer exposed to a solution of eggPC + 10% DOTAP (1.25 mM) lipid vesicles in PBS. (c) Percent change in the amplitude of the FFT peak in a (corresponding to the index contrast at the $pSiO_2$ layer/solution interface) as a function of time for the same sample.

that neither the vesicles nor their lipid constituents entered the $pSiO_2$ layer, consistent with previous results.[22] Upon longer exposures to the buffer solution (either with or without added vesicles), the value of $2nL$ was observed to undergo a slight continuous decrease ascribed to the slow dissolution of the $pSiO_2$ film.

Figure 3c displays the variation of the amplitude of the FFT peak from the $pSiO_2$ film exposed to eggPC + 10% DOTAP vesicles as a function of time. This profile qualitatively matches the simulation presented in Figure 2: upon introduction of the lipid vesicles, the amplitude of the FFT peak is observed to decrease abruptly (within 5 min), as indicated by A–B in Figure 3c. In the simulation, this drop corresponds to the adsorption of a single layer of lipid vesicles onto the surface of $pSiO_2$. The importance of electrostatic interactions between vesicles and the substrate and lipid bilayer formation have been

dx.doi.org/10.1021/la301085t | Langmuir XXXX, XXX, XXX–XXX

established in the literature. For example, neutral or only slightly charged PC SUVs adsorb to silica or mica surfaces as intact vesicles, which then subsequently decompose into lipid bilayers. By contrast, SUVs made of positively charged lipids (DOTAP) rupture immediately upon encountering negatively charged surfaces such as silica.[15−17] In the present case, the simulation indicates that instantaneous rupture of the vesicles upon adsorption to the $pSiO_2$ surface should not result in an abrupt decrease in the intensity of the FFT signal. Thus, the experimental data indicate that the vesicles adsorb to the $pSiO_2$ surface as intact vesicles. The adsorption of intact vesicles at the surface of $pSiO_2$ continues to a point where a second regime is started, when the amplitude of the FFT peak reaches a relatively constant value (region B−C in Figure 3c). Consistent with the results of Kasemo and co-workers using SPR and QCM measurements, this regime is ascribed to the initiation of vesicle rupture and bilayer formation.[16] The transition from vesicles to a bilayer requires the continuous adsorption of new vesicles from solution in order to supply sufficient lipid to complete the bilayer. In our experimental case, the relatively flat appearance of the curve in region B−C in Figure 3c most likely results from a competition between the two processes of vesicle adsorption and bilayer formation. The simulations performed in the present work did not accommodate simultaneous vesicle adsorption and lipid bilayer formation. Subsequent to the initial adsorption event, the amplitude of the FFT peak fluctuates in response to local changes in the refractive index contrast at the $pSiO_2$ surface (C−D in Figure 3c) as a result of the coexistence of vesicles adsorbed to the surface with yet-formed lipid bilayers.

It should be pointed out that processes such as deformation of the adsorbed lipid vesicles at the $pSiO_2$ surface and/or the fusion of vesicles to each other prior to rupturing and forming a lipid bilayer cannot be excluded.[8]

Upon flushing the system with pure PBS buffer, a prompt increase in the signal amplitude is observed (region D in Figure 3c). This is attributed to the removal of the extra vesicles still present at the $pSiO_2$ surface. The FFT signal does not recover to the value it displayed in pure buffer prior to vesicle introduction, and this is attributed to the lipid bilayer remaining at the surface of the $pSiO_2$ film and to some vesicles also remaining at the $pSiO_2$ surface after the system was flushed. AFM and fluorescence imaging experiments have confirmed the presence of the lipid bilayer after the sample rinsing step (data not shown). The percentage changes observed in the experimental data were ~4 times larger than predicted by the simulations, which may be due to the adsorption of additional lipids or vesicles remaining within voids or cracks in the top few nanometers of the $pSiO_2$ film.

Control experiments on thin mica sheets were performed to test the validity of the above interpretations of the optical data. Vesicle deposition and bilayer formation on flat mica surfaces have been well described and characterized in the literature.[5,7,8] The mica used in the present experiments was sufficiently transparent that when cleaved to a thickness of a few tens of micrometers it displayed interference fringes in the reflectivity spectrum analogous to those observed from the $pSiO_2$ films. Both the mica and the $pSiO_2$ samples possess a net negative surface charge. Unlike the $pSiO_2$ samples, mica is not porous; consequently, effects observed in the optical reflectivity spectrum from mica can be exclusively ascribed to phenomena occurring at the surface of the film. The unilamellar lipid vesicle formulation used in the $pSiO_2$ experiments (eggPC + 10% DOTAP, low positive charge for the lipid vesicles, 1.25 mM concentration of vesicles, 100 nm nominal diameter, and room-temperature exposure) is known to adsorb first as vesicles and then rupture into bilayers on a mica surface.[7]

Films of mica were exposed to a lipid solution of the same composition (eggPC + 10% DOTAP) as was employed in the $pSiO_2$ experiments. The interference spectrum of the mica film in PBS and the FFT of the interference spectrum are presented in Figure 4a and in the inset of Figure 4a, respectively. Figures

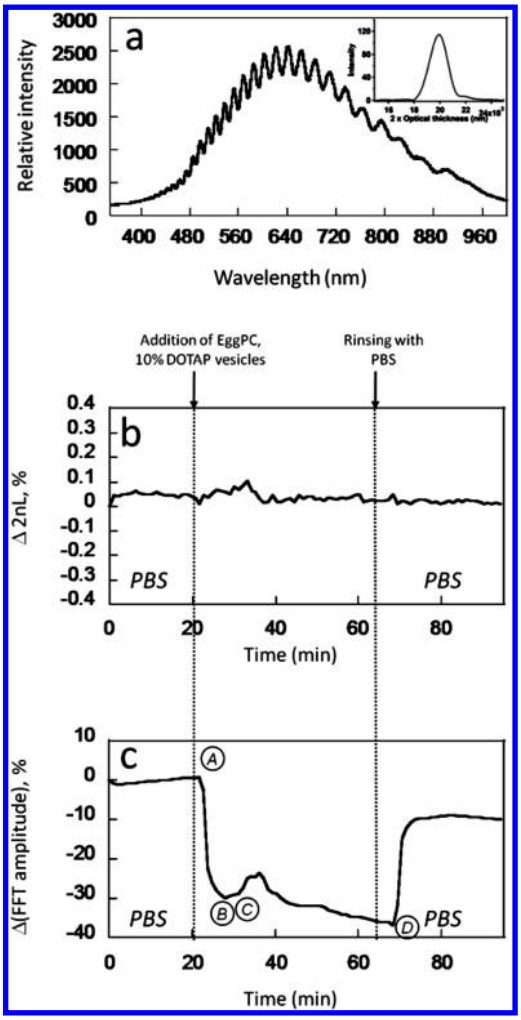

Figure 4. Experimental RIFTS data for a mica film exposed to an eggPC + 10% DOTAP lipid solution. (a) Reflected light spectrum displaying interference fringes from a thin film of mica. The sample is immersed in a pure PBS solution. (Inset) Fourier transform of the spectrum in a. The FFT spectrum displays a single peak whose position along the x axis corresponds to $2nL$ for the mica film. (b) Value of $2nL$ as a function of time for mica film exposed to a solution of eggPC + 10% DOTAP (1.25 mM) lipid vesicles in PBS. (c) Percent change in the amplitude of the FFT peak from a (corresponding to the index contrast at the mica/solution interface) as a function of time for the same sample.

4b,c display the variation of the quantity $2nL$ and the amplitude of the FFT peak as a function of time after the addition of a solution of vesicles prepared from eggPC and 10% DOTAP.

As expected, the position of the FFT peak (value of $2nL$) does not change after the addition of the lipid vesicles (Figure 4b) because the mica layer is not porous. However, the amplitude of the FFT peak undergoes pronounced changes as

dx.doi.org/10.1021/la301085t | *Langmuir* XXXX, XXX, XXX−XXX

the vesicle layer adsorbs and decomposes into a lipid bilayer (Figure 4c). A sharp decrease in amplitude is observed in the first 5 min of exposure (denoted by A−B in Figure 4c) as lipid vesicles adsorb to the mica surface. This result duplicates the experimental $pSiO_2$ data, and is consistent with the results given by the simulations. Subsequent to the initial adsorption event, the amplitude of the FFT peak fluctuates in response to local changes in the refractive index contrast at the mica surface (C−D in Figure 4c), presumably because of the evolution of the lipid bilayer as was previously observed with this type of lipid on mica.[7,8] The optical response is quite similar in form and magnitude to that observed on the $pSiO_2$ sample (Figure 3d), and it suggests that vesicle rupture and bilayer formation follow similar pathways on these two surface types. Note that the observed decrease in the amplitude of the FFT peak (which reports the index contrast at the interface) is larger than what is predicted by the simulations for the adsorption of a single monolayer of vesicles or a single lipid bilayer. To be consistent with the simulation calculations, the surface could contain a stack of 5−10 lipid bilayers at the interface along with adsorbed vesicles. Because of the relatively large fraction of water contained in the vesicles, the index contrast that could be achieved at an interface containing a multilayer of vesicles can provide a change in amplitude, Δ(FFT amplitude), of only ∼14% (Figure 2d), not the ∼30% change observed in the $pSiO_2$ and mica data (Figures 3c and 4c, respectively). Thus, the stacking of extra vesicle layers on mica is less likely than the possible rupture of the eggPC and DOTAP vesicles to form one or more bilayers, consistent with prior literature observations.[8,11] The optical measurement in the present work probes a much larger area (1 mm^2) than a typical AFM measurement, providing an average value of the index contrast. Thus, it is also possible that the lipid layers are heterogeneous, with patches of multiple lipid bilayers scattered on the sample otherwise containing single bilayers. On both mica and $pSiO_2$, the formation of a lipid bilayer, under our experimental conditions, includes two steps: (i) vesicle adsorption and (ii) the rupture of adsorbed vesicles to form a bilayer once a critical vesicular coverage has been achieved. The data indicate that the second step occurs approximately simultaneous with the first, ∼5 min after the introduction of the vesicle solution.

To determine if in the above hypothesis the large percentage change in the FFT signal amplitude is due to the buildup of lipid bilayers on the sample surface, an experiment was performed in which $pSiO_2$ was exposed to a PBS solution containing 1.25 mM DPPC (dipalmitoylphosphatidylcholine) vesicles. Unlike vesicles made from eggPC, DPPC vesicles do not rupture into bilayers at room temperature. Indeed, with a phase-transition temperature of 41 °C, DPPC is in a gel phase at room temperature.

Figure 5 displays the time dependence of the position of the FFT peak (value of $2nL$) and the amplitude of the FFT peak upon addition of the stable DPPC vesicles. As was observed with eggPC + 10% DOTAP vesicles, no variation in the value of $2nL$ is observed, apart from the gradual decrease due to the slow dissolution of the $pSiO_2$ sample (Figure 5a). Thus, we conclude that no DPPC vesicles or their constituents enter the pores of the $pSiO_2$ film. The amplitude of the FFT peak is observed to decrease by 15% (A−B in Figure 5b), in agreement with the simulation for the adsorption of a single monolayer of DPPC vesicles. After the initial response, the FFT amplitude signal is stable, showing none of the fluctuations observed in either the $pSiO_2$ or mica experiments when eggPC + 10% DOTAP vesicles were used (B−C of Figure 5b). The lack of signal fluctuations in the B−C region supports the interpretation that this behavior is indicative of vesicle rupture and adsorption of a lipid bilayer at the optical sensor surface. The adsorption of vesicles to the surface, referred to as step 3 in Figure 1, appears to be the only adsorption process in the case of DPPC vesicles. This is consistent with the expectation that bilayer formation from vesicle rupture is not favorable to DPPC at room temperature. When the sample is rinsed with PBS, the FFT amplitude signal recovers slightly, stabilizing at a Δ(FFT amplitude) value of 12−12.5%. Presumably, this recovery is due to the removal of small quantities of excess vesicles, present as a second or third layer on the $pSiO_2$ surface in the B−C region.

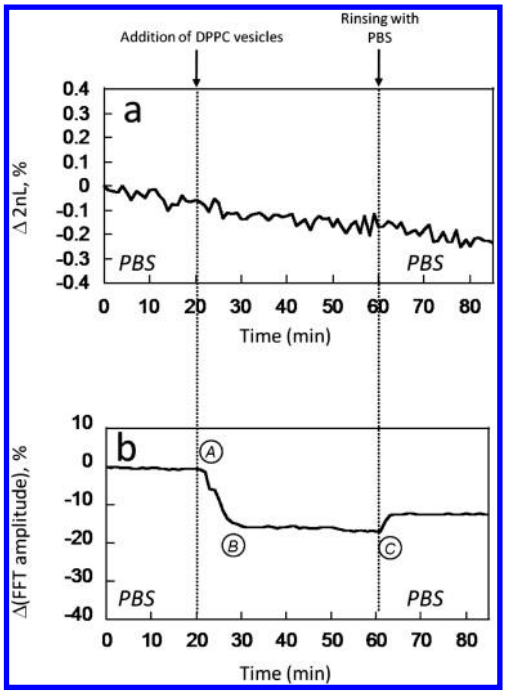

Figure 5. Experimental RIFTS data for an oxidized $pSiO_2$ film exposed to a DPPC lipid solution. (a) Value of $2nL$ as a function of time for the $pSiO_2$ layer exposed to a solution of DPPC (1.25 mM) lipid vesicles in PBS. (b) Percent change in the amplitude of the FFT peak (corresponding to the index contrast at the $pSiO_2$ layer/solution interface) as a function of time for the same sample.

The ability of the RIFTS method to distinguish between intact and disrupted vesicles means that it should be useful in the study of processes that trigger such events. The porous nature of the $pSiO_2$ material may be useful in this regard; the loading and release of many types of proteins and drugs has been achieved in porous silicon,[32−44] so the pores of the material could be used as nanoscale reservoirs for membrane disrupting or transporting agents.

CONCLUSIONS

The RIFTS method provides a sensitive means to monitor the adsorption and evolution of vesicles and lipids at optical surfaces in real time. The method works equally well on flat (mica) or porous (mesoporous Si) substrates, and it can distinguish between simple vesicle adsorption (in the case of DPPC vesicles) and vesicle disruption events that form phospholipid bilayers (eggPC + 10%DOTAP vesicles). It is sensitive to the index contrast in the near vicinity (<200 nm) of an optical interface. The interpretation of the experimental data

dx.doi.org/10.1021/la301085t | Langmuir XXXX, XXX, XXX−XXX

is supported by optical simulations, illustrating the possible steps in the vesicle-to-bilayer transformation process. The simulation established that vesicle deposition at the surface of $pSiO_2$ or mica yields a decrease in the interfacial refractive index contrast, which results in a decrease in the amplitude of the peak observed in the fast Fourier transform of the reflected-light spectrum. Because of the larger refractive index of a lipid bilayer relative to that of a vesicle (on a volumetric basis), the deposition of multiple lipid bilayers can generate relatively large changes in the amplitude of the FFT signal. Because RIFTS can also monitor the infiltration of lipid molecules into the voids of the mesoporous Si film, the experiments established that no significant infiltration of lipid molecules occurred with the samples used in this study.

■ ASSOCIATED CONTENT

Supporting Information

Additional information on the deposition of phospholipid bilayers, optical fluorescence microscopy, and atomic force microscopy for this work. This material is available free of charge via the Internet at http://pubs.acs.org

■ AUTHOR INFORMATION

Corresponding Author

*E-mail: frederique.cunin@enscm.fr. Tel: +33 4 67 16 34 44. Fax: +33 4 67 16 34 70.

Present Address

[⊥]Institut Européen des Membranes, UMR5635, 300 Avenue du Professeur E. Jeanbrau, 34 095, Montpellier, France.

Notes

The authors declare no competing financial interest.

■ ACKNOWLEDGMENTS

This material is based upon work supported in part by the U.S. National Science Foundation under grant no. DMR-0806859 and by the CNRS-DREI under grant no. 3312. Frederic Pichot at ATEMI (University Montpellier 2) is acknowledge for the design of the mask on the silicon wafers.

■ REFERENCES

(1) Bagatolli, L. A. To see or not to see: lateral organization of biological membranes and fluorescence microscopy. *Biochim. Biophys. Acta. Biomembr.* **2006**, *1758*, 1541−1556.

(2) Pfeiffer, I.; Seantier, B.; Petronis, S.; Sutherland, D.; Kasemo, B.; Zaech, M. Influence of nanotopography on phospholipid bilayer formation on silicon dioxide. *J. Phys. Chem. B* **2008**, *112*, 5175−5181.

(3) Rossi, C.; Chopineau, J. Biomimetic tethered lipid membranes designed for membrane-protein interaction studies. *Eur. Biophys. J. Biophys. Lett.* **2007**, *36*, 955−965.

(4) Sackmann, E. Supported membranes: scientific and practical applications. *Science* **1996**, *271*, 43.

(5) Seantier, B.; Giocondi, M. C.; Le Grimellec, C.; Milhiet, P. E. Probing supported model and native membranes using AFM. *Curr. Opin. Colloid Interface Sci.* **2008**, *13*, 326−337.

(6) Tanaka, M S. Polymer-supported membranes as models of the cell surface. *Nature* **2005**, *437*, 656−663.

(7) Reviakine, I.; Brisson, A. Formation of supported phospholipid bilayers from unilamellar vesicles investigated by atomic force microscopy. *Langmuir* **2000**, *16*, 1806−1815.

(8) Goksu, E. I.; Vanegas, J. M.; Blanchette, C. D.; Lin, W. C.; Longo, M. L. AFM for structure and dynamics of biomembranes. *Biochim. Biophys. Acta, Biomembr.* **2009**, *1788*, 254−266.

(9) Dong, S.; Chen, X. Some new aspects in biosensors. *J. Biotechnol.* **2002**, *82*, 303−323.

(10) Sinner, E. K.; Ritz, S.; Naumann, R.; Schiller, S.; Knoll, W. Self-assembled tethered bimolecular lipid membranes. *Adv. Clin. Chem.* **2009**, *49*, 159−179.

(11) Richter, R. P.; Brisson, A. Following the formation of supported lipid bilayers on mica: a study combining AFM, QCM-D, and ellipsometry. *Biophys. J.* **2005**, *88*, 3422−3433.

(12) Keller, C. A.; Kasemo, B. Surface specific kinetics of lipid vesicle adsorption measured with a quartz crystal microbalance. *Biophys. J.* **1998**, *75*, 1397−1402.

(13) Seantier, B.; Breffa, C.; Félix, O.; Decher, G. Dissipation-enhanced quartz crystal microbalance studies on the experimental parameters controlling the formation of supported lipid bilayers. *J. Phys. Chem. B* **2005**, *109*, 21755−21765.

(14) Richter, R. P.; Bérat, R.; Brisson, A. R. Formation of solid-supported lipid bilayers: an integrated view. *Langmuir* **2006**, *22*, 3497−3505.

(15) Richter, R.; Mukhopadhyay, A.; Brisson, A. Pathways of lipid vesicle deposition on solid surfaces: a combined QCM-D and AFM study. *Biophys. J.* **2003**, *85*, 3035−3047.

(16) Keller, C. A.; Glasmastar, K.; Zhdanov, V. P.; Kasemo, B. Formation of supported membranes from vesicles. *Phys. Rev. Lett.* **2000**, *84*, 5443−5446.

(17) Keller, C. A.; Kasemo, B. Surface specific kinetics of lipid vesicle adsorption measured with a quartz crystal microbalance. *Biophys. J.* **1998**, *75*, 1397−1402.

(18) Jane, A.; Dronov, R.; Hodges, A.; Voelcker, N. H. pSi biosensors on the advance. *Trends Biotechnol.* **2009**, *27*, 230−239.

(19) Pacholski, C.; Sartor, M.; Sailor, M. J.; Cunin, F.; Miskelly, G. M. Biosensing using pSi double-layer interferometers: reflective interferometric Fourier transform spectroscopy. *J. Am. Chem. Soc.* **2005**, *127*, 11636−11645.

(20) Sailor, M. J. Porous Silicon in Practice: Preparation, Characterization, and Applications. Wiley-VCH: Weinheim, Germany, 2012; pp 152−156.

(21) Sailor, M. J.; Link., J. R. "Smart dust": nanostructured devices in a grain of sand. *Chem. Commun.* **2005**, *11*, 1375−1383.

(22) Cunin, F.; Milhiet, P. E.; Anglin, E.; Sailor, M. J.; Espenel, C.; Le Grimellec, C.; Brunel, D.; Devoisselle, J. M. Continuous planar phospholipid bilayer supported on pSi thin film reflector. *Ultramicroscopy* **2007**, *107*, 1048−1052.

(23) Worsfold, O.; Voelcker, N. H.; Nishiya, T. Biosensing using lipid bilayers suspended on pSi. *Langmuir* **2006**, *22*, 7078−7083.

(24) McLeod, H. A. *Thin-Film Optical Filters*; Adam Hilger Ltd: Bristol, U.K.,1986; p49.

(25) Lang, H.; Duschl, C.; Gratzel, M.; Vogel., H. Self-assembly of thiolipid molecular layers on gold surfaces: optical and electrochemical characterization. *Thin Solid Films* **1992**, *210/211*, 818−821.

(26) Johnson, S. J.; Bayerl, T. M.; McDermott, D. C.; Adam, G. W.; Rennie, A. R.; Thomas, R. K.; Sackmann, E. Structure of an adsorbed dimyristoylphosphatidylcholine bilayer measured with specular reflection of neutrons. *Biophys. J.* **1991**, *59*, 289−294.

(27) Johnson, S. J.; Bayerl, T. M.; Weihan, W.; Noack, H.; Penfold, J.; Thomas, R. K.; Kanellas, D.; Rennie, A. R.; Sackmann, E. Coupling of spectrin and polylysine to phospholipid monolayers studied by specular reflection of neutrons. *Biophys. J.* **1991**, *60*, 1017−1025.

(28) Seantier., B.; Breffa, C.; Félix, O.; Decher, G. In Situ Investigations of the formation of mixed supported lipid bilayers close to the phase transition temperature. *Nano Lett.* **2004**, *4*, 5−10.

(29) Burns, A. R.; Frankel, D. J.; Buranda, T. Local mobility in lipid domains of supported bilayers characterized by atomic force microscopy and fluorescence correlation spectroscopy. *Biophys. J.* **2005**, *89*, 1081−1093.

(30) Chiantia, S.; Kahya, N.; Ries, J.; Schwille, P. Effects of ceramide on liquid-ordered domains investigated by simultaneous AFM and FCS. *Biophys. J.* **2006**, *90*, 4500−4508.

(31) Milhiet, P. E.; Le Grimellec, C. Observing the Nanoscale Organization of Model Biological Membranes by Atomic Force Microscopy. In *Life at the Nanoscale*; Dufrene, Y. F., Ed.; Pan Stanford Publishing: Singapore, 2011; Vol. *1*, pp 1−20.

(32) Wu, E. C.; Andrew, J. S.; Buyanin, A.; Kinsella, J. M.; Sailor, M. J. Suitability of porous silicon microparticles for the long-term delivery of redox-active therapeutics. *Chem. Commun.* **2011**, *47*, 5699−5701.
(33) Wu, E. C.; Andrew, J. S.; Cheng, L.; Freeman, W. R.; Pearson, L.; Sailor, M. Real-time monitoring of sustained drug release using the optical properties of porous silicon photonic crystal particles. *J. Biomater.* **2011**, *32*, 1957−1966.
(34) Andrew, J. S.; Anglin, E. J.; Wu, E. C.; Chen, M. Y.; Cheng, L.; Freeman, W. R.; Sailor, M. J. Sustained release of a monoclonal antibody from electrochemically prepared mesoporous silicon oxide. *Adv. Funct. Mater.* **2010**, *20*, 4168−4174.
(35) Wu, E. C.; Park, J.-H.; Park, J.; Segal, E.; Cunin, F.; Sailor, M. J. Oxidation-triggered release of fluorescent molecules or drugs from mesoporous Si microparticles. *ACS Nano* **2008**, *2*, 2401−2409.
(36) Orosco, M. M.; Pacholski, C.; Sailor, M. J. Real-time monitoring of enzyme activity in a mesoporous silicon double layer. *Nat. Nanotechnol.* **2009**, *4*, 255−258.
(37) Wang, M.-J.; Coffer, J. L.; Dorraj, K.; Hartman, P. S.; Loni, A.; Canham, L. T. Sustained antibacterial activity from triclosan-loaded nanostructured mesoporous silicon. *Mol. Pharmaceutics* **2010**, *7*, 2232−2239.
(38) Dongmei; Loni, A.; Canham, L. T.; Coffer, J. L. Location-dependent controlled release kinetics of model hydrophobic compounds from mesoporous silicon/biopolymer composite fibers Fan. *Phys. Status Solidi A* **2009**, *206*, 1322−1325.
(39) Mukherjee, P.; Whitehead, M. A.; Senter, R. A.; Fan, D.; Coffer, J. L.; Canham, L. T. Biorelevant mesoporous silicon/polymer composites: directed assembly, disassembly, and controlled release. *Biomed. Microdev.* **2006**, *8*, 9−15.
(40) Santos, H. A.; Salonen, J.; Bimbo, L. M.; Lehto, V.-P.; Peltonen, L.; Hirvonen, J. Mesoporous materials as controlled drug delivery formulations. *J. Drug Delivery Sci. Technol.* **2011**, *21*, 139−155.
(41) Kilpelainen, M.; Monkare, J.; Vlasova, M. A.; Riikonen, J.; Lehto, V.-P.; Salonen, J.; Jarvinen, K.; Herzig, K.-H. Nanostructured porous silicon microparticles enable sustained peptide (Melanotan II) delivery. *Eur. J. Pharm. Biopharm.* **2011**, *77*, 20−25.
(42) Kilpelaeinen, M.; Moenkaere, J.; Riikonen, J.; Vlasova, M.; Salonen, J.; Lehto, V. P.; Herzig, K. H.; Jaervinen, K. Mesoporous silicon microparticles as carriers for peptides. *J. Controlled Release* **2010**, *148*, e43−e44.
(43) Kashanian, S.; Harding, F.; Irani, Y.; Klebe, S.; Marshall, K.; Loni, A.; Canham, L.; Fan, D.; Williams, K. A.; Voelcker, N. H. Evaluation of mesoporous silicon/polycaprolactone composites as ophthalmic implants. *Acta Biomater.* **2010**, *6*, 3566−357.
(44) Jiang, K.; Loni, A.; Canham, L. T; Coffer, J. L. Incorporation and characterization of boron neutron capture therapy agents into mesoporous silicon and silicon nanowires. *Phys. Status Solidi A* **2009**, *206*, 1361−1364.